

Hamiltonian Monte Carlo-Based Near-Optimal MIMO Signal Detection

Junichiro Hagiwara, *Member, IEEE*, Toshihiko Nishimura, *Member, IEEE*, Takanori Sato, *Member, IEEE*, Yasutaka Ogawa, *Life Fellow, IEEE*, and Takeo Ohgane, *Member, IEEE*

Abstract—Multiple-input multiple-output (MIMO) technology is essential for the optimal functioning of next-generation wireless networks; however, enhancing its signal-detection performance for improved spectral efficiency is challenging. Here, we propose an approach that transforms the discrete MIMO detection problem into a continuous problem while leveraging the efficient Hamiltonian Monte Carlo algorithm. For this continuous framework, we employ a mixture of t -distributions as the prior distribution. To improve the performance in the coded case further, we treat the likelihood’s temperature parameter as a random variable and address its optimization. This treatment leads to the adoption of a horseshoe density for the likelihood. Theoretical analysis and extensive simulations demonstrate that our method achieves near-optimal detection performance while maintaining polynomial computational complexity. This MIMO detection technique can accelerate the development of 6G mobile communication systems.

Index Terms—Hamiltonian Monte Carlo, horseshoe distribution, Markov chain Monte Carlo (MCMC), Multiple-input multiple-output (MIMO), prior distribution, signal detection, t -distribution, temperature parameter.

I. INTRODUCTION

THE widespread adoption of 5G networks underscores the pivotal role of wireless communications in contemporary infrastructure. Ongoing 6G research aims to enhance user experience by improving the utilization efficiency of the radio spectrum. The multiple-input multiple-output (MIMO) technology is crucial for the effective utilization of the radio spectrum in next-generation wireless networks. By employing multiple antennas at both ends, MIMO systems significantly boost the efficiency of wireless transmission. Although conventional MIMO systems have been widely implemented, recent studies have focused on massive MIMO systems [2].

High-accuracy signal detection in MIMO systems is crucial for enhancing their overall transmission efficiency. Generally, the maximum likelihood detection algorithm delivers optimal performance; however, its exhaustive search approach and

Manuscript received xx yy, 2024. This paper was presented in part at the GLOBECOM 2023, Kuala Lumpur, Malaysia, 4–8 December 2023 [1] (DOI: 10.1109/GLOBECOM54140.2023.10437162).

Junichiro Hagiwara was with the Faculty of Information Science and Technology, Hokkaido University, Sapporo 060-0814, Japan. He is currently with the Faculty of Social Informatics, Mukogawa Women’s University, Nishinomiya 663-8558, Japan (e-mail: hagijyun@gmail.com).

Toshihiko Nishimura, Takanori Sato, Yasutaka Ogawa, and Takeo Ohgane are with the Faculty of Information Science and Technology, Hokkaido University, Sapporo 060-0814, Japan (e-mail: nishim@ist.hokudai.ac.jp; tk-sato@ist.hokudai.ac.jp; ogawa@ist.hokudai.ac.jp; ohgane@ist.hokudai.ac.jp).

Color versions of one or more of the figures in this paper are available online at <http://ieeexplore.ieee.org>.

associated computational costs limit its practical application in MIMO systems [3]. Linear-detection algorithms, such as the minimum mean-square error (MMSE) algorithm, offer computational efficiency but underperform compared to optimal techniques [3]. The key challenge lies in enhancing the signal-detection accuracy without exceeding the practical computational limits. A promising approach involves adopting a stochastic framework for MIMO signal detection. This perspective enables the theoretical incorporation of uncertainty and the application of advanced probabilistic methods in signal processing.

Stochastic approaches, including Bayesian methods, have been applied to improve the MIMO signal detection [4], [5]. Continuous prior distributions are generally considered unsuitable for MIMO signal detection, with the exception of [6] and our previously proposed methods [1], [7]–[13]. In the mixed Gibbs sampling (MGS) method [14], numerous samples are employed to approximate the posterior distribution based on discrete prior distribution and Gibbs sampling [15], a Markov chain Monte Carlo (MCMC) technique. To improve MCMC exploration with discrete prior distribution, [16] introduces the dynamic scaling of the likelihood’s temperature parameter, which impacts the Gibbs sampling exploration. Alternatively, [17], [18] suggest a Metropolis–Hastings algorithm utilizing the likelihood gradient information. Furthermore, the expectation propagation (EP) method [19] employs a discrete prior distribution and applies the EP algorithm [20] to approximate the posterior distribution parameters. Most stochastic MIMO detection studies have adopted a discontinuous prior distribution, reflecting the discrete nature of the transmission symbols. Consequently, numerous powerful algorithms designed for continuous problems are not being fully leveraged, limiting the advancement of MIMO signal detection research.

Our approach transforms the MIMO signal detection from a discrete problem to a continuous one, utilizing the efficient Hamiltonian Monte Carlo (HMC) method [21]. We adopt a mixture of t -distributions as the prior distribution [1] for this continuous framework. Notably, [6] also employs a continuous prior distribution similar to that in our proposed method; however, they adopt the Langevin algorithm for the posterior distribution approximation. The Langevin algorithm can be considered a special case of HMC where the Hamiltonian equations are solved numerically for only one step [22]. Consequently, while [6] prioritizes computational efficiency, our proposed method focuses on the detection accuracy.

Furthermore, we consider a detection method for our approach in cases when channel coding, which is commonly

employed in practical wireless communications, is applied. To improve the coded performance, we integrate signal detection with error-correction decoding synergistically. Additionally, the likelihood's temperature parameter is considered a random variable, enabling automatic optimization. This treatment extends the likelihood from a normal density to a horseshoe [23] one, as the temperature parameter follows a Cauchy distribution.

Theoretical analysis and simulations demonstrate our method's near-optimal detection performance with polynomial computational complexity. Our innovative MIMO detection technique advances both the practical and theoretical domains of next-generation wireless networks.

This study builds upon the work of [1]. The primary enhancement is the application of channel coding, which entailed implementing substantial adaptations to the original framework. Additionally, we conduct a detailed study to explain why the proposed method achieves better performance with the modulation order.

This paper is organized as follows: Section II introduces the problem's stochastic formulation. Section III provides an overview of MGS and EP, two established stochastic methods. Sections IV and V detail the proposed approach for the uncoded and coded scenarios, respectively. Section VI presents the outcomes of the theoretical analysis and numerical simulations. Section VII concludes the paper with a summary of the key points.

The key notations utilized in this paper are presented below. \mathbb{C} represents the complex number field. $\text{Re}(\mathbf{x})$ and $\text{Im}(\mathbf{x})$ indicate \mathbf{x} 's real and imaginary components, respectively. $\hat{\mathbf{x}}$ represents the estimated value of \mathbf{x} . $E[\mathbf{x}]$ denotes the expectation of \mathbf{x} . $\|\mathbf{x}\|$ represents the Euclidean norm of \mathbf{x} . $\mathbf{0}$ and \mathbf{I} represent the zero vectors and the identity matrix, respectively. \mathbf{X}^\top indicates the transpose of matrix \mathbf{X} . $\lfloor x \rfloor$ signifies the floor function, the largest integer less than or equal to x . \sim indicates that the left-side random variable follows the right-side probability distribution. The proportionality between quantities is represented by \propto .

II. PROBLEM FORMULATION

A. System Model

We examine a full-stream MIMO configuration featuring N -transmitting and M -receiving antennas (Fig. 1). This MIMO system is described by the following relationship:

$$\mathbf{y} = \mathbf{H}\mathbf{u} + \mathbf{w}, \quad \mathbf{w} \sim \mathcal{CN}(\mathbf{0}, \sigma_w^2 \mathbf{I}), \quad (1)$$

where $\mathbf{y} = [y_1, \dots, y_M]^\top \in \mathbb{C}^M$ denotes the received symbol vector, $\mathbf{H} \in \mathbb{C}^{M \times N}$ is the channel matrix, $\mathbf{u} = [u_1, \dots, u_N]^\top \in \mathbb{C}^N$ represents the transmission symbol vector, $\mathbf{w} = [w_1, \dots, w_M]^\top \in \mathbb{C}^M$ denotes the noise vector with variance σ_w^2 , and \mathcal{CN} denotes a circularly symmetric complex normal distribution. For computation convenience, we decompose the complex numbers into real and imaginary parts as follows: $\mathbf{y} \rightarrow \begin{bmatrix} \text{Re}(\mathbf{y}) \\ \text{Im}(\mathbf{y}) \end{bmatrix}$, $\mathbf{H} \rightarrow \begin{bmatrix} \text{Re}(\mathbf{H}) & -\text{Im}(\mathbf{H}) \\ \text{Im}(\mathbf{H}) & \text{Re}(\mathbf{H}) \end{bmatrix}$, $\mathbf{u} \rightarrow \begin{bmatrix} \text{Re}(\mathbf{u}) \\ \text{Im}(\mathbf{u}) \end{bmatrix}$, and $\mathbf{w} \rightarrow \begin{bmatrix} \text{Re}(\mathbf{w}) \\ \text{Im}(\mathbf{w}) \end{bmatrix}$. Note that the vector and matrix characters remain the same when N and M are doubled to $2N$ and $2M$,

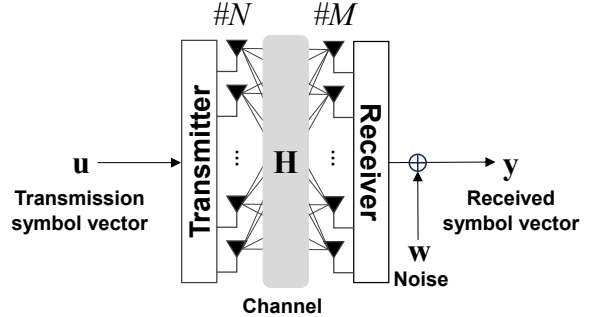


Fig. 1. System model.

respectively. In this study, we presume that the channel matrix \mathbf{H} and noise variance σ_w^2 are known. Additionally, we assume that scramblers ensure the uniformly random transmission of symbols across the antennas, with known average power P_t . The goal of signal detection is to estimate the transmitted symbol vector \mathbf{u} from the received symbol vector \mathbf{y} .

From the stochastic perspective, Bayes' theorem (posterior distribution \propto likelihood \times prior distribution) yields

$$p(\mathbf{u} | \mathbf{y}) \propto p(\mathbf{y} | \mathbf{u})p(\mathbf{u}). \quad (2)$$

Therefore, stochastic signal detection aims to derive a point estimate from the posterior distribution $p(\mathbf{u} | \mathbf{y})$.

B. Likelihood

Equation (1) demonstrates the following relationship:

$$p(\mathbf{y} | \mathbf{u}) = \mathcal{N}(\mathbf{y}; \mathbf{H}\mathbf{u}, \sigma_w^2 \mathbf{I}), \quad (3)$$

where \mathcal{N} denotes the probability density of a real-valued normal distribution. σ_w represents the average noise amplitude. In physics, this term is also referred to as the temperature parameter [24]. When using MCMC to approximate posterior distributions, this value is sometimes intentionally altered from the original. This is because it strongly influences the estimation. However, it is generally difficult to optimize this parameter [24].

C. Prior Distribution

The prior distribution, as shown in (2), can be interpreted as a regularization term that calibrates the likelihood. We can combine multiple prior distributions for different purposes. For example, when applying two independent prior distributions simultaneously, we define them separately as $p_1(\mathbf{u})$ and $p_2(\mathbf{u})$ and subsequently consider their product, $p(\mathbf{u}) = p_1(\mathbf{u})p_2(\mathbf{u})$. Similarly, this study considers multiple types of prior distributions, which will be explained in detail.

The primary and essential prior distributions in signal detection represent the signal position, denoted as $p_1(\mathbf{u})$. For MIMO signal detection, a discrete multinomial prior distribution is commonly employed to represent potential discrete signal points. This approach enhances the posterior estimation accuracy by prioritizing the transmission signal points, as shown in (4) (see Fig. 2 (a)):

$$p_1(\mathbf{u}) = \prod_{n=1}^{2N} \frac{1}{q} \{ \delta(u_n - a_1) + \dots + \delta(u_n - a_q) \}, \quad (4)$$

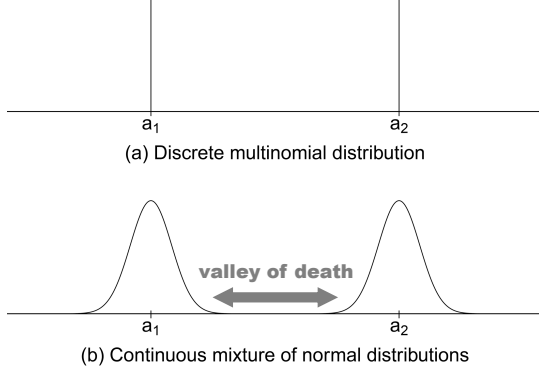


Fig. 2. Two examples of priors for binary phase-shift keying (BPSK).

where q represents the modulation order's square root, a_1, \dots, a_q are the real-valued signal point coordinates, and $\delta(x)$ is the unit probability mass at x . Both the MGS and EP methods incorporate this form of prior distribution in their signal-detection processes.

Adopting a continuous prior distribution converts the discrete problem into a continuous problem. Equation (5) illustrates this approach using a mixture of normal distributions (see Fig. 2 (b)):

$$p_1(\mathbf{u}) = \prod_{n=1}^{2N} \frac{1}{q} \{ \mathcal{N}(u_n; a_1, \sigma) + \dots + \mathcal{N}(u_n; a_q, \sigma) \}, \quad (5)$$

where σ^2 represents the normal distribution variance of each component, a crucial tuning parameter. In our prior work [7]–[13], we employed this type of prior distribution, optimizing σ to minimize the bit error rate (BER) via preliminary searches. The optimal σ value represents an equilibrium point that maximizes search efficiency. An overly high σ value reduces search efficiency as irrelevant areas beyond the transmission signal points are explored. Conversely, a very low σ value limits component distribution overlap, hindering exploration across different signal points (the “valley of death” in Fig. 2 (b)).

Next, we may consider a secondary prior distribution to mitigate the noise enhancement effect [3] in MIMO signal detection. This prior distribution, denoted as $p_2(\mathbf{u})$, is a wide normal distribution centered at zero, whose effect is often referred to as ridge regularization [25]:

$$p_2(\mathbf{u}) = \mathcal{N}(\mathbf{u}; \mathbf{0}, \sigma_{\text{ridge}}^2 \mathbf{I}), \quad (6)$$

where σ_{ridge} is a tuning parameter. If we set $p(\mathbf{u}) = p_2(\mathbf{u})$ alone, the posterior distribution can be derived analytically. In this case, the mean of the posterior distribution becomes the well-known MMSE solution in the average setting $\sigma_{\text{ridge}}^2 = P_t$:

$$\begin{aligned} p(\mathbf{u} | \mathbf{y}) &\propto p(\mathbf{y} | \mathbf{u})p(\mathbf{u}) \\ &= \mathcal{N}(\mathbf{y}; \mathbf{H}\mathbf{u}, \sigma_w^2 \mathbf{I})\mathcal{N}(\mathbf{u}; \mathbf{0}, P_t \mathbf{I}) = \mathcal{N}(\mathbf{u}; \boldsymbol{\mu}, \boldsymbol{\Sigma}), \end{aligned} \quad (7)$$

where $\boldsymbol{\mu} = \mathbf{H}^\top \mathbf{y}$ and $\boldsymbol{\Sigma} = (\mathbf{H}^\top \mathbf{H} + \sigma_w^2 / P_t \mathbf{I})^{-1}$.

D. Posterior Distribution

Assuming a mixture distribution as the prior distribution prevents closed-form analytical solutions for the posterior

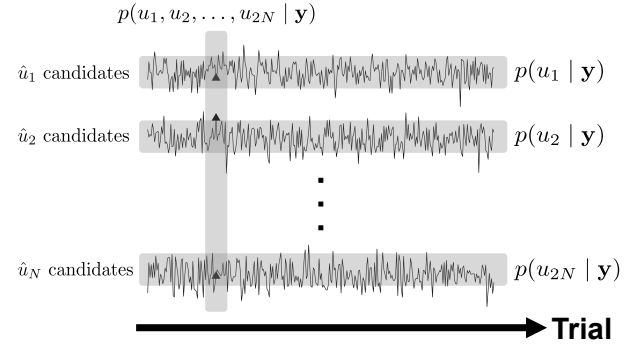


Fig. 3. Criteria for selecting a single one from soft-value symbol candidates.

distribution [26]. Deriving the posterior distribution requires numerical approximation algorithms. The point estimate of the posterior distribution, $\hat{\mathbf{u}}$, may yield various candidates based on the chosen approximation algorithm. Moreover, $\hat{\mathbf{u}}$ might deviate from the actual transmission signal point. A continuous prior distribution may lead to explorations outside the discrete signal points, inducing potential deviations in the estimates.

To address these issues, from the candidates for the soft-value symbol $\hat{\mathbf{u}}$, we select a single one according to a certain criterion and quantize it to the nearest signal point if a hard decision is needed. We can consider several criteria for selecting the finalist. The primary approach lies in the joint posterior distribution $p(u_1, u_2, \dots, u_{2N} | \mathbf{y})$ (see Fig. 3). First, we calculate the likelihood $p(\mathbf{y} | \hat{\mathbf{u}})$ for each quantized $\hat{\mathbf{u}}$ from $\hat{\mathbf{u}}$. Thereafter, we select the $\hat{\mathbf{u}}$ corresponding to the $\hat{\mathbf{u}}$ which yields the highest likelihood. We refer to this as the joint posterior-based point estimator. The secondary approach lies in the marginal posterior distribution $p(u_n | \mathbf{y})$ (see Fig. 3). We select the set $\{E[u_1 | \mathbf{y}], E[u_2 | \mathbf{y}], \dots, E[u_{2N} | \mathbf{y}]\}$ as the finalist. We refer to this as the marginal posterior-based point estimator. Generally, while the joint distribution contains detailed information, it is averaged out during marginalization. Therefore, although estimation should ideally be based on the joint distribution, the well-behaved marginal distribution can also be beneficial under noisy conditions. We primarily employ the joint posterior-based point estimator, while also employing the marginal posterior-based point estimator, depending on the situation.

III. PREVIOUS WORK

A. MGS Method [14]

The MGS method estimates the posterior distribution through extensive sample generation. It utilizes Gibbs sampling, focusing on areas with high posterior probability densities. The MGS method enhances efficiency by refreshing the initial search values with the $1/(2N)$ probability, thereby avoiding local optima traps. With this approach, the Markov chains are virtually parallelized. Additionally, [14] proposes a multiple restarts technique, which runs several MGS processes with varied initial Markov chain values and thereafter selects the highest likelihood result. Sufficient restarts are demonstrated to achieve near-optimal performance. However,

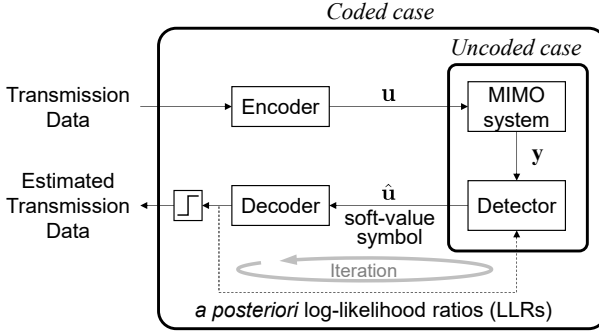


Fig. 4. System diagram for the uncoded and coded cases.

as highlighted in [27], the performance degrades significantly as the modulation order increases.

The MGS method's complexity per Markov chain step is $\mathcal{O}(2M2N)$, primarily due to the likelihood computation. The overall complexity becomes $\mathcal{O}(L_{\text{MGS}}2M2N)$, where L_{MGS} represents the total Markov chain steps.

B. EP Method [19]

The EP method estimates the posterior distribution with an uncorrelated multivariate normal distribution $q(\mathbf{u})$. The method uses the EP algorithm to find parameters that minimize $-\int p(\mathbf{u} \mid \mathbf{y}) \ln\{q(\mathbf{u})/p(\mathbf{u} \mid \mathbf{y})\} d\mathbf{u}$, the Kullback–Leibler divergence. The approach iteratively refines the mean and variance parameters, using the final mean to estimate the transmitted symbols. [19] suggests setting the total number of iterations L_{EP} to at most 10 to achieve optimal detection performance. As mentioned in [26], the EP algorithm does not always guarantee convergence. Thus, we employ damping in our implementation to enforce convergence stability, as described in [19].

The per-iteration complexity of the EP method is $\mathcal{O}((2N)^3)$, primarily due to its internal matrix inversion operation. The final complexity reaches $\mathcal{O}(10(2N)^3)$ with total iterations $L_{\text{EP}} = 10$.

IV. PROPOSED SIGNAL DETECTION FOR THE UNCODED CASE

A. System Diagram

Fig. 4 shows the system diagram of the proposed detector. The inner part represents the uncoded case, where the input is \mathbf{u} and the output is a soft-value symbol $\hat{\mathbf{u}}$ (finalist). For hard decisions, the output is quantized to the nearest constellation point.

B. Likelihood

For the uncoded case, the likelihood is given by (3).

C. Prior Distribution

For the uncoded case, we assume that $p(\mathbf{u}) = p_1(\mathbf{u})$ by considering only the primary $p_1(\mathbf{u})$.

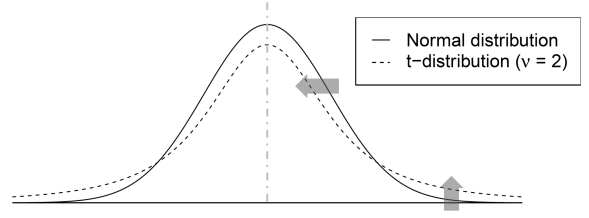


Fig. 5. Normal and t -distributions with identical location and scale parameters.

We adopt a mixture of t -distributions as the prior distribution for signal position, expressed in (8):

$$p_1(\mathbf{u}) = \prod_{n=1}^{2N} \frac{1}{q} \{ \mathcal{T}(u_n; a_1, \sigma, \nu) + \dots + \mathcal{T}(u_n; a_q, \sigma, \nu) \}, \quad (8)$$

where \mathcal{T} represents a real-valued t -distribution density [26] with tunable parameters σ (scale) and ν (degrees of freedom). We utilize the optimal values for these parameters, determined through preliminary searches. The t -distribution features a sharper peak and heavier tails than the normal distribution with identical location and scale parameters (see Fig. 5). Consequently, t -distributions enable a more exhaustive exploration around the transmission signal points than normal distributions. Furthermore, they facilitate the exploration of other potential signal points by traversing the inter-point valley of death. This approach offers superior exploration compared to our previous normal distribution mixture [7]–[13].

D. Posterior Distribution

In the uncoded case, we consider only the primary joint posterior-based point estimator.

Next, we focus on algorithms that numerically approximate the posterior distribution. Signal detection using a continuous prior distribution leads to a continuous posterior distribution, attributed to the continuous likelihood. This allows the use of powerful continuous-domain algorithms for the posterior distribution approximation. Previously, we evaluated Newton's method, automatic differentiation variational inference (ADVI [28]), and HMC as approximation algorithms using normal mixture priors [11]. The results indicated HMC's superior signal-detection performance at comparable computational complexities. HMC's auxiliary momentum variables, randomly redrawn at each Markov chain step, appear to mitigate the local optima issues often encountered in Newton's method and ADVI. Therefore, we utilize the HMC method to approximate the posterior distribution in our research.

HMC, an MCMC variant, employs Markov chain principles similar to the MGS method. Therefore, HMC samples regions with high posterior probability densities to approximate the posterior distribution. The sampling efficiency of HMC typically surpasses those of other MCMC methods, attributed to its innovative application of Hamiltonian mechanics. The key aspects of the HMC method are outlined below. First, the HMC introduces an auxiliary momentum variable $\mathbf{r} = d\mathbf{u}/d\tau$, where τ denotes virtual time, alongside the estimated variable \mathbf{u} . Further, the method considers the potential energy $U(\mathbf{u}) =$

Algorithm 1 HMC sampling

```

1: Initialize  $\mathbf{u}$  at random
2: for  $l = 1, \dots, L_{\text{HMC}}$  do
3:   Draw  $\mathbf{r}$  from  $\mathcal{N}(\mathbf{0}, \mathbf{I})$ 
4:   Numerically solve Hamilton's equations (10) to obtain  $\mathbf{u}'$  and  $\mathbf{r}'$ 
5:   Update  $\mathbf{u} \leftarrow \mathbf{u}'$  with probability  $\min[1, \exp\{H(\mathbf{u}, \mathbf{r}) - H(\mathbf{u}', \mathbf{r}')\}]$ 
6:   Regard the updated  $\mathbf{u}$  as a sample from the posterior distribution
    $p(\mathbf{u} \mid \mathbf{y})$ 
7: end for

```

$-\ln(p(\mathbf{u} \mid \mathbf{y}))$ and kinetic energy $K(\mathbf{r}) = 1/2\|\mathbf{r}\|^2$. The Hamiltonian representing the total system energy is defined as

$$H(\mathbf{u}, \mathbf{r}) = U(\mathbf{u}) + K(\mathbf{r}). \quad (9)$$

Hamilton's equations are now formulated as two partial differential equations:

$$\begin{aligned} \frac{d\mathbf{u}}{d\tau} &= \frac{\partial H(\mathbf{u}, \mathbf{r})}{\partial \mathbf{r}} = \mathbf{r}, \\ \frac{d\mathbf{r}}{d\tau} &= -\frac{\partial H(\mathbf{u}, \mathbf{r})}{\partial \mathbf{u}} = -\frac{\partial U(\mathbf{u})}{\partial \mathbf{u}}. \end{aligned} \quad (10)$$

Algorithm 1 illustrates the HMC sampling process. The Hamiltonian remains constant according to (9). Consequently, the substantial changes in the momentum \mathbf{r} significantly impact the sample value \mathbf{u} . Meanwhile, Algorithm 1 shows that most proposals (\mathbf{u}') are accepted with a probability of one, except for numerical error cases. These features contribute to HMC's superior sampling efficiency compared to those of other MCMC methods.

Incidentally, we verify the actual behavior of the HMC through an example. Fig. 6 shows an example of the sample-value trajectories during the estimation of the three BPSK symbols, using a mixture t -distribution as the prior distribution. The x-axis of each panel represents the number of Markov chain steps (i.e., the number of “dice rolls”). Different-colored chains indicate distinct Markov chains operating in parallel. Fig. 6 demonstrates that HMC conducts concentrated exploration around symbol positions, albeit with some overshoots and undershoots.

Algorithm 1 implies that solving (10) numerically in one Markov chain step involves L internal evaluations of the log-posterior density derivative. While L may vary with the problem, we typically assumed $L = 10$ in this study, following an example in [29]. The computational complexity of the HMC method is primarily determined by the term $(\mathbf{H}^\top \mathbf{H})\mathbf{u}$. This term emerges from the log-likelihood component in the differentiation of the log-posterior probability density. Since \mathbf{H} is known, $(\mathbf{H}^\top \mathbf{H})$ only needs to be computed once. Consequently, the HMC's per-step computational complexity is $\mathcal{O}(L(2N)^2) = \mathcal{O}(10(2N)^2)$. The total complexity, given L_{HMC} Markov chain steps, becomes $\mathcal{O}(10L_{\text{HMC}}(2N)^2)$.

V. PROPOSED SIGNAL DETECTION FOR THE CODED CASE

A. System Diagram

Fig. 4 shows the system diagram of the proposed detector. The inner uncoded case is expanded to the outer coded case by incorporating an encoder and a decoder. Error correction

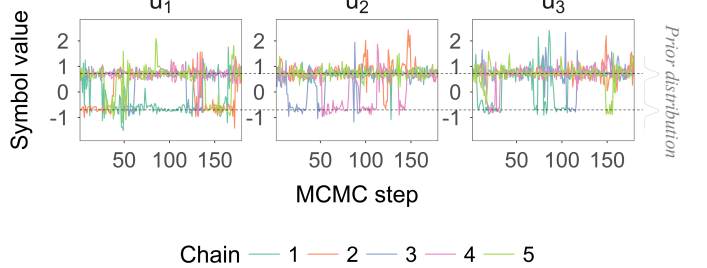


Fig. 6. Actual example of the HMC behavior.

is achieved using turbo codes [30], which have a proven track record in 4G/5G. The decoder's input is the soft-value symbol $\hat{\mathbf{u}}$ (finalist) from the detector, based on the posterior distribution. The decoder's output is bit-wise *a posteriori* log-likelihood ratios (LLRs), which are the final values after the turbo decoding internal iterations. Feeding these LLRs back to the detector enables iterative detection and decoding, which enhances estimation performance [16], [31]. Accordingly, we employ the LLR feedback approach in this study. While the initial detection and decoding do not involve LLR feedback, joint detection and decoding with the LLR feedback are implemented in subsequent phases.

B. Likelihood

In the coded case, we consider an extension of (3) for the joint detection and decoding with LLR feedback. This extension aims to further enhance the performance of our proposed method utilizing the LLR.

As mentioned earlier, when using MCMC to approximate the posterior distribution, we can improve the detection performance by intentionally modifying the temperature parameter from the average noise amplitude. However, this optimization task is generally challenging. Therefore, this study proposes treating the temperature parameter as a random variable for automatic optimization. Specifically, we extend the formulation through multiplying the average noise amplitude by a positive coefficient:

$$\sigma_w \rightarrow \lambda_n \sigma_w. \quad (n = 1, \dots, 2N) \quad (11)$$

Here, we consider λ_n to be an independent random variable. This approach maintains the average noise amplitude as a reference while easily accommodating significantly different values when necessary. Henceforth, let $\boldsymbol{\lambda} = [\lambda_1, \dots, \lambda_{2N}]^\top$.

We can assume various probability distributions for λ_n . The most basic one is a uniform distribution limited to positive supports. However, uniform distributions may lead to insufficient estimation performance when computational resources are finite. This is because all positive regions are explored with equal weight. We propose using a Cauchy distribution as follows:

$$\lambda_n \sim \mathcal{C}^+(0, \sigma_{\text{Cauchy}}), \quad (12)$$

where \mathcal{C}^+ denotes a Cauchy distribution limited to positive supports, with the location parameter 0 and the scale parameter σ_{Cauchy} . The optimal value for σ_{Cauchy} is determined through preliminary searches. Under this setup, the likelihood

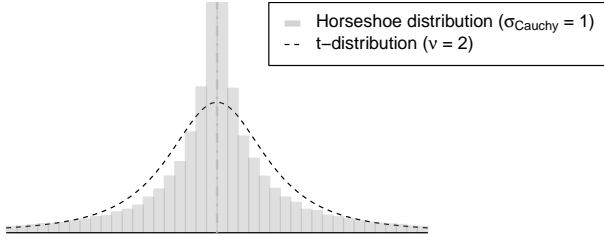


Fig. 7. Horseshoe and t -distributions with identical location and scale parameters.

extends from $p(\mathbf{y} \mid \mathbf{u})$ to $p(\mathbf{y} \mid \mathbf{u}, \boldsymbol{\lambda})$, which follows a normal density. Consequently, the standard $p(\mathbf{y} \mid \mathbf{u})$, after marginalizing $\boldsymbol{\lambda}$ out, follows a horseshoe density [23]. Fig. 7 shows the horseshoe and t -distributions with identical location and scale parameters. As analytical expressions are impossible for representing the horseshoe distribution [23], it is displayed using simulated frequencies. The horseshoe distribution, characterized by a thin peak and heavy tails, is suitable for our problem. It typically takes values around a specific value but occasionally produces significantly deviant values. This distribution enables targeted exploration around the peak (near average noise amplitude) and the tails (far from average noise amplitude). Thus, it is expected to enhance the exploration efficiency when computational resources are finite, improving the estimation performance. Originally, the horseshoe distribution was proposed as a prior distribution for the regression coefficients in sparse regression [23]. In this study, however, we apply it to the likelihood rather than the prior distribution for transmission symbols.

The introduction of the new random variable λ_n increases the computational complexity compared with that in the uncoded case. Processing $\boldsymbol{\lambda}$ in the likelihood within the HMC framework incurs $\mathcal{O}(2N)$ additional operations per step, accounting for their mutual independence. Nevertheless, this additional load is insignificant compared to the previously clarified per-step complexity of $\mathcal{O}(10(2N)^2)$ for the uncoded case. Therefore, this increase does not substantially affect the total computational expenditure.

C. Prior Distribution

As described in Section V-B, in the coded case, we may consider $\boldsymbol{\lambda}$ in addition to \mathbf{u} . In this case, the prior distribution is extended from $p(\mathbf{u})$ to $p(\mathbf{u}, \boldsymbol{\lambda})$. Since \mathbf{u} and $\boldsymbol{\lambda}$ are mutually independent, $p(\mathbf{u}, \boldsymbol{\lambda}) = p(\mathbf{u}) \times p(\boldsymbol{\lambda})$. For $p(\mathbf{u})$, we consider $p_1(\mathbf{u})$ and $p_2(\mathbf{u})$, setting $p(\mathbf{u}) = p_1(\mathbf{u})p_2(\mathbf{u})$. Here, $p_1(\mathbf{u})$ is extended from (8) to accommodate the LLR feedback from the decoder. $p_2(\mathbf{u})$ is introduced to improve the performance at low signal-to-noise ratios (SNRs). Furthermore, when considering $\boldsymbol{\lambda}$, we include an additional prior distribution $p(\boldsymbol{\lambda})$ based on (12).

First, regarding $p_1(\mathbf{u})$, the term $1/q$ in (8) implies that an equal occurrence frequency is adopted for each symbol. To consider joint detection and decoding with the LLR feedback, we extend the definition of $p_1(\mathbf{u})$ to express the uneven symbol

occurrence frequencies:

$$p_1(\mathbf{u}) = \prod_{n=1}^{2N} \{\omega_1 \mathcal{T}(u_n; a_1, \sigma, \nu) + \dots + \omega_q \mathcal{T}(u_n; a_q, \sigma, \nu)\}, \quad (13)$$

where $\sum_{l=1}^q \omega_l = 1$. Although ω_l is set to $1/q$ for the initial detection, it becomes an LLR-dependent value for the subsequent joint detection and decoding. The relationship between ω_l and the LLR feedback from the decoder is described below. Let the bit sequence representation of a symbol be $b_1 \dots b_r \dots b_R$. Here, $R = \log_2 q$. Given that the LLR for b_r is denoted as Λ_r , where $\Lambda_r := \ln \frac{p(b_r=1|\mathbf{y})}{p(b_r=0|\mathbf{y})} = \ln \frac{p(\mathbf{y}|b_r=1)}{p(\mathbf{y}|b_r=0)}$, we obtain the following equations:

$$p(b_r = '0' \mid \mathbf{y}) = 1/(1 + e^{\Lambda_r}), \quad (14)$$

$$p(b_r = '1' \mid \mathbf{y}) = e^{\Lambda_r}/(1 + e^{\Lambda_r}). \quad (15)$$

Therefore, we can obtain the weight ω_l by multiplying (14) and (15) according to the bit sequence of the l th symbol. For 16QAM, $R = \log_2 \sqrt{16} = 2$, yielding the bit sequence $b_1 b_2$. For a symbol with the bit sequence $b_1 b_2 = 01$, the weight is $p(b_1 = '0' \mid \mathbf{y})p(b_2 = '1' \mid \mathbf{y})$.

Next, we set the variance parameter in $p_2(\mathbf{u})$ given by (6) as follows:

$$\sigma_{\text{ridge}}^2 = \sigma_w^2 / [\max\{\text{SVD}(\mathbf{H})\}^2 / \lambda_{\text{ridge}}], \quad (16)$$

where $\text{SVD}(\mathbf{H})$ represents the singular values of \mathbf{H} , and $\lambda_{\text{ridge}} > 1$ is a constant. The optimal value of λ_{ridge} is determined through preliminary searches. Unlike MMSE, wherein σ_{ridge}^2 is set to the average transmission power P_t , our method depends on σ_w and \mathbf{H} . This improves the adaptability to the SNR and individual channels, enhancing the detection performance.

Finally, when considering $\boldsymbol{\lambda}$, we include

$$p(\boldsymbol{\lambda}) = \prod_{n=1}^{2N} p(\lambda_n) = \prod_{n=1}^{2N} \mathcal{C}^+(\lambda_n; 0, \sigma_{\text{Cauchy}}) \quad (17)$$

based on (12).

The introduction of $p_2(\mathbf{u})$ and $p(\boldsymbol{\lambda})$ increases the computational complexity compared to the complexity recorded in the uncoded case. The most computationally intensive aspect in $p_2(\mathbf{u})$ is deriving the singular values. We need to perform this calculation only once initially because we assume that the \mathbf{H} is known. This calculation typically adds $\mathcal{O}(2M2N \times \min\{2M, 2N\})$ operations. However, as we will discuss later, our study sets $L_{\text{HMC}} = 1000$ and $N = M = 96$. Compared to the total computational complexity of $\mathcal{O}(10L_{\text{HMC}}(2N)^2)$ for the uncoded case, this increase can be considered negligible. Regarding $p(\boldsymbol{\lambda})$, the additional per-step complexity within the HMC is $\mathcal{O}(2N)$, due to the mutual independence of λ_n . However, this increase is negligible compared to the previously identified per-step computational complexity of $\mathcal{O}(10(2N)^2)$ for the uncoded case. Therefore, it does not dominate the overall computational cost.

D. Posterior Distribution

In the coded case, in addition to the joint posterior-based point estimator, we consider the marginal posterior-based

TABLE I
COMMON ASSUMPTIONS IN NUMERICAL ANALYSES

Item	Setting
Trials	5000 transmission symbol vectors (uncoded) and 100 codewords (coded)
Number of antennas	$N = M = 96$
Modulation order	Quadrature phase-shift keying (QPSK), 16 quadrature-amplitude modulation (QAM), and 64QAM
Symbol mapping	Gray code
Average transmission power	$P_t = 1/2$
Fading	Quasi-static Rayleigh
Channel correlation	Kronecker model (correlation coefficient $\rho = 0$)
Channel coding	Uncoded and coded cases

point estimator. Specifically, we apply the marginal posterior-based point estimator for the initial detection without the LLR feedback. We employ the joint posterior-based point estimator for subsequent joint detection and decoding with the LLR feedback. This approach aims to improve the detection performance at low SNRs in the initial phase without LLR assistance. In subsequent phases, the approach aims to achieve the best estimation with the highest likelihood aided by the LLR.

To approximate the posterior distribution, we apply the effective HMC algorithm, as in the uncoded case.

Notably, when considering λ , the joint posterior extends from $p(\mathbf{u} | \mathbf{y})$ to $p(\mathbf{u}, \lambda | \mathbf{y})$. Our main objective remains the estimation of \mathbf{u} . λ serves only as the auxiliary variable for improving the estimation accuracy. Thus, we consider $p(\mathbf{u} | \mathbf{y})$ as the joint posterior, marginalizing out λ^1 . This marginalization can be achieved simply by discarding the λ samples obtained simultaneously, thereby maintaining the computational complexity.

VI. NUMERICAL RESULTS AND DISCUSSION

Our proposed technique achieves near-optimal MIMO signal detection while maintaining the polynomial computational complexity. We validate these claims through theoretical complexity analyses and extensive signal-detection simulations.

A. Settings in Numerical Analysis

1) *Common Assumptions*: The study considers the typical conditions for massive MIMO systems, as shown in Table I. Furthermore, we configured the turbo encoding and decoding settings, as shown in Table II. These settings ensure that the error-correction code delivers appropriate performance. BER plots are excluded for simulations yielding error-free results.

2) *Parameters of Proposed Method*: Parameters σ and ν for t -distribution, σ_{Cauchy} for Cauchy distribution, and λ_{ridge} for ridge regularization were optimized via a preliminary search (see Table III). Aligned with the virtual parallelization concept in the MGS method, we configured each simulated Markov chain to comprise $2N$ steps. The number of parallel Markov chains was set to $\lfloor 1000/(2N) \rfloor$, ensuring sufficient

¹That is, $p(\mathbf{u} | \mathbf{y}) = \int p(\mathbf{u}, \lambda | \mathbf{y}) d\lambda \propto \int p(\mathbf{y} | \mathbf{u}, \lambda) p(\mathbf{u}, \lambda) d\lambda = \int p(\mathbf{y} | \mathbf{u}, \lambda) p(\lambda | \mathbf{u}) p(\mathbf{u}) d\lambda = \int p(\mathbf{y} | \mathbf{u}, \lambda) p(\lambda) d\lambda \times p(\mathbf{u}) = p(\mathbf{y} | \mathbf{u}) \times p(\mathbf{u}) = \text{horseshoe likelihood} \times \mathbf{u}'s \text{ prior.}$

TABLE II
CHANNEL CODING AND DECODING SETTINGS

Item	Setting
Turbo coding	Constituent recursive systematic convolutional coding <ul style="list-style-type: none"> constraint length: 4 rate: 1/2
Interleaving	Random bit interleaving
Turbo decoding	Constituent decoding <ul style="list-style-type: none"> algorithm: maximum <i>a posteriori</i> (MAP) iterations: 10
Code rate	1/3
Code length [bits]	6144 (QPSK and 16QAM) and 6336 (64QAM)

TABLE III
PARAMETERS DETERMINED THROUGH THE PRELIMINARY SEARCH

	Mixture of t -distributions		σ_{Cauchy}	λ_{ridge}
	σ	ν		
QPSK	0.1242	1.8	2.0	15
16QAM	0.0621	1.8	5.0	62
64QAM	0.0531	2.5	3.0	230

performance [1]. This configuration results in a total of approximately 1000 Markov chain steps, equivalent to L_{HMC} .

3) *Parameters of Existing Stochastic Methods*: For the MGS method, we set $L_{\text{MGS}} = 1000$ Markov chain steps, matching L_{HMC} in our proposed method. The proposed method, however, incurs 10 times higher computational complexity than the MGS method, attributed to its internal numerical evaluation process ($L = 10$). For equitable comparison, we implemented 10 multiple restarts in the MGS method.

Additionally, we configured the EP method with $L_{\text{EP}} = 10$ iterations, which is adequate for achieving satisfactory performance.

4) *Well-known Benchmark Methods*: We consider the MMSE method as a representative MIMO linear-detection method.

In addition, the MIMO detection efficiency is often measured against single-input single-output (SISO) transmissions with additive white Gaussian noise (AWGN), owing to its freedom from cross-antenna interference and channel fading. The BER performance of the SISO AWGN serves as a crucial reference for evaluating the MIMO detection performance.

B. Computational Complexity

For signal detection, our proposed method, MGS, and EP methods exhibit complexities of $\mathcal{O}(10 \times 1000(2N)^2)$, $10 \times \mathcal{O}(1000(2N)^2)$, and $\mathcal{O}(10(2N)^3)$, respectively, with $N = M$. All of these methods demonstrate polynomial-order computational complexities. Our proposed and MGS methods have an identical complexity, whereas the EP method is the most computationally efficient, given $N = 96 (< 1000/2)$.

C. Uncoded BER Performance: Proposed Method vs. Linear MMSE Method (Fig. 8 (a) Through (c))

The proposed method significantly outperforms the MMSE method at moderate-to-high SNRs for all modulation orders. This confirms the advantage of our nonlinear processing method over linear methods. However, the proposed method

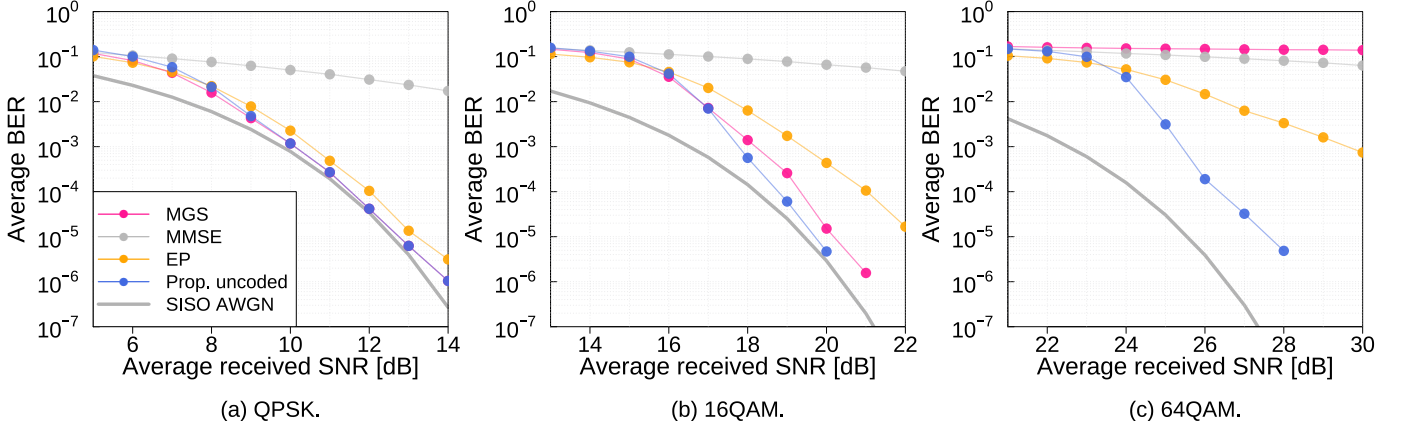


Fig. 8. Uncoded case: average BER versus average received SNR.

performs equally or slightly worse at low SNRs for all modulation orders. The factors causing performance degradation at low SNR and their countermeasures are discussed in Sections VI-F and VI-G.

D. Uncoded BER Performance: Proposed Method vs. Existing Stochastic Methods

1) *Overall Trend (Fig. 8 (a) Through (c))*: Increasing the modulation order results in greater performance divergence from the SISO AWGN benchmarks. Higher modulation orders expand the signal constellations, reducing inter-point distances and complicating the signal estimation processes.

2) *Comparison for QPSK (Fig. 8 (a))*: The performances of all the examined stochastic methods are closely aligned with that of the SISO AWGN, showing slight variations. The simplicity of signal detection resulting from the sparse transmission points and wide inter-point spacing for the QPSK contributes to this similarity in performance. Under low SNR conditions, our proposed method exhibits slightly inferior performance compared to the MGS and EP methods. Sections VI-F and VI-G explore low SNR performance decline factors and remedies. At moderate-to-high SNRs, our proposed method surpasses the EP method and matches the MGS method in terms of performance. At 10^{-3} BER, our proposed method achieves SNR gains of approximately 0 dB and 0.4 dB over the MGS and EP methods, respectively.

3) *Comparison for 16QAM (Fig. 8 (b))*: The 16QAM scenario, unlike QPSK, features denser signal constellations and reduced inter-point spacings, complicating its detection process. Such a challenging environment highlights the distinct features of individual detection methods. Unlike the case in the QPSK scenario, our proposed method achieves the best detection performance at moderate-to-high SNRs. The performance gap between our proposed method and the existing stochastic methods widens at high SNRs compared to the case in the QPSK scenarios. At 10^{-3} BER, our method achieves SNR gains of 0.4 dB over the MGS method and 1.6 dB over the EP method.

4) *Comparison for 64QAM (Fig. 8 (c))*: The 64QAM scenario presents the most complex signal-detection condition, which highlights the unique capabilities of our proposed

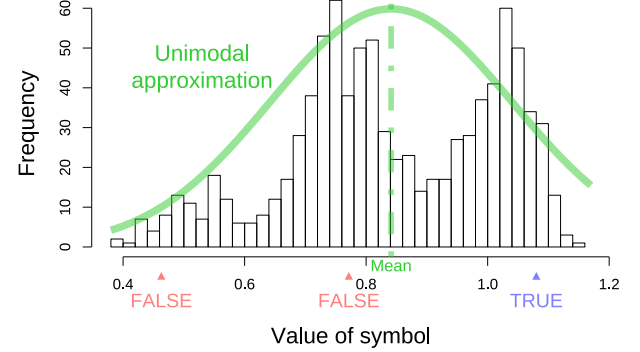


Fig. 9. Histogram of the marginal posterior distribution for a certain symbol (64QAM and SNR = 25 dB).

method more than the QPSK or 16QAM scenario. This complexity stems from the 64QAM's highly dense constellation and minimal inter-point spacing. Unlike the case in the QPSK and 16QAM scenarios, our proposed method surpasses the MGS method in terms of performance at low SNRs. Our proposed method excels at moderate-to-high SNRs, as is the case in the 16QAM scenario. Furthermore, in the 64QAM scenario, our performance advantage over existing stochastic methods becomes more pronounced. At 10^{-3} BER, our proposed method demonstrates an immeasurably large SNR gain over the MGS method and a 4.2-dB improvement compared with the results of the EP method.

Here, based on a specific example, we explain why the performance advantage of the proposed method relatively grows with the modulation order. This trend is related to the ability of the method to express multimodality in the posterior distribution. The EP method assumes a unimodal multivariate normal distribution for the approximate posterior distribution. In contrast, our simulation-based method can capture the posterior distribution as it is, thus expressing multimodality. Fig. 9 shows a histogram of the marginal posterior distribution for a certain symbol where the BER performance differs. In difficult estimation scenarios, the posterior distribution becomes multimodal as multiple possibilities for the transmission symbols remain plausible, as shown in this example. Forcibly approximating such a distribution with a unimodal

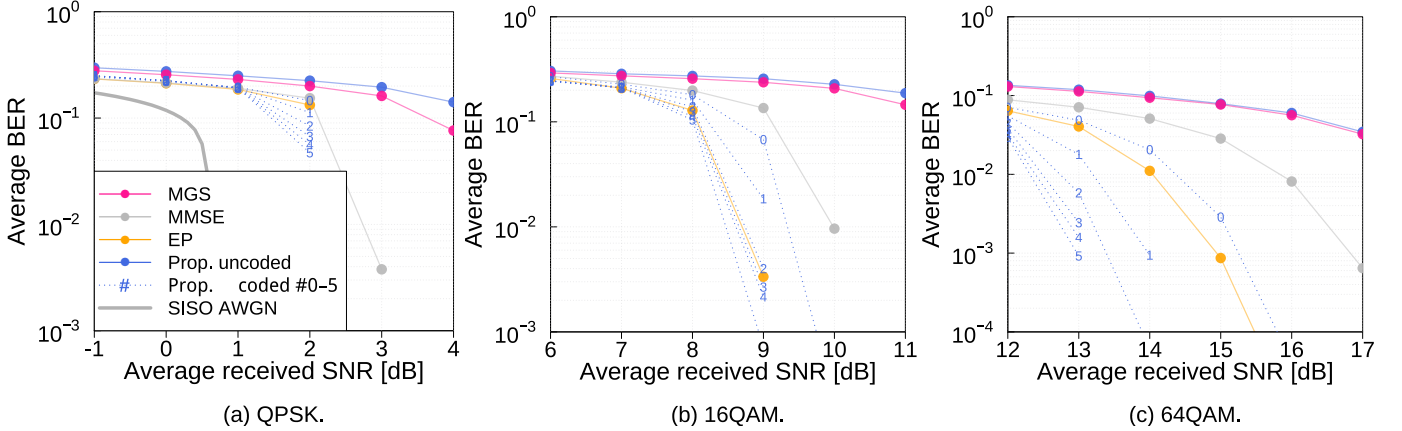


Fig. 10. Coded case: average BER versus average received SNR.

distribution can lead to erroneous symbol estimations. That is, the unimodal peak may shift incorrectly due to the influence of the wrong symbol possibilities. The proposed method can select the result with the maximum likelihood among multiple modes, enabling correct symbol estimation and improving the detection performance. Such a situation becomes more likely as the number of candidate transmission symbols increases. Thus, the effectiveness of the proposed method increases with the modulation order. The ability to express multimodality in the posterior distribution is a common feature of simulation-based methods, including the MGS method. However, in this simulation environment, the MGS method demonstrates a lower detection performance relative to the proposed method. This is attributed to the inferior search capability of the MGS method at high modulation orders, where MCMC tends to stall, as discussed in [27].

E. Uncoded BER Performance: Proposed Method vs. SISO AWGN (Fig. 8 (a) Through (c))

Our proposed method exhibits near-optimal performance for signal detection in the uncoded case. At 10^{-3} BER, the SNR degradation for our method remains below 0.3, 1.3, and 2.9 dB in the QPSK, 16QAM, and 64QAM scenarios, respectively. This remarkable efficacy stems from a well-tuned prior distribution configuration coupled with an efficient search algorithm. Our prior distribution closely approximates the discrete point mass at the transmission signals while facilitating the exploration of alternative signal points. The HMC algorithm employed in our method ensures effective sampling even in complex signal-detection scenarios. Our proposed method exhibits high reliability given its exceptional performance and sound methodological foundation.

F. Coded BER Performance: Initial Detection and Decoding Without LLR Feedback (Fig. 10 (a) Through (c))

For reference, we first present the results obtained by simply applying error-correction codes to the previous uncoded method (“Prop. uncoded” in Fig. 10). Based on the results, the proposed method exhibits the worst performances. This is due to its poor performance at low SNRs in the uncoded

case. Therefore, we consider improving the performance of the proposed method at low SNRs. The relatively good performances of the MMSE and EP methods provide insights for this improvement.

The MMSE results suggest that ridge regularization, which mitigates noise enhancement, is effective in noisy situations. Therefore, we introduce an additional prior distribution $p_2(\mathbf{u})$.

The EP method estimates the transmitted symbols using the mean of a unimodal marginal posterior distribution. This feature is a disadvantage in the ambiguous estimation scenarios at moderate-to-high SNRs, as shown in Fig. 9. However, the average estimates may be advantageous at low SNRs. Consequently, we change the point estimator of the posterior distribution to the marginal posterior-based point estimator.

Considering the above, we set the prior distribution as $p(\mathbf{u}) = p_1(\mathbf{u})p_2(\mathbf{u})$. Additionally, we adopt a marginal posterior-based point estimator for the posterior distribution. The BER performances labeled “Prop. coded #0” in Fig. 10 display the results under these conditions. This approach achieves performance better than that of the MMSE method and closer to that of the EP method in the waterfall region for all modulation orders.

G. Coded BER Performance: Subsequent Joint Detection and Decoding With LLR Feedback (Fig. 10 (a) Through (c))

Here, we consider further improving the coded performance of the proposed method using the LLR feedback.

In the likelihood, the temperature parameter exerts a strong influence on the MCMC estimation. We treat it as a random variable for automatic optimization. Specifically, we handle the likelihood as the horseshoe density, as shown by (11) and (12). Notably, if λ_n in (11) followed a uniform distribution unlike in (12), the detection performance would have deteriorated. Further details regarding the uniform distribution case are provided in Appendix A.

For the prior distribution, we introduce $p_2(\mathbf{u})$ and $p(\boldsymbol{\lambda})$ as additional priors. $p_2(\mathbf{u})$ is introduced because ridge regularization remains effective, as in initial detection and decoding without LLR feedback. $p(\boldsymbol{\lambda})$ emerges as a consequence of introducing the new random variable λ_n .

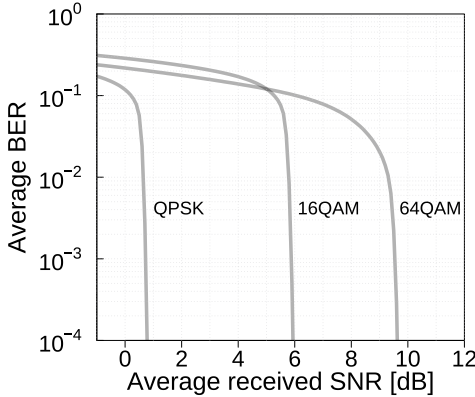


Fig. 11. Coded BER performances of SISO AWGN.

Regarding the posterior distribution, we adopt the joint posterior-based point estimator to achieve the best estimation with the highest likelihood leveraging LLR feedback.

Considering the above, we present the BER performances (“Prop. coded #1–5” in Fig. 10) under the following conditions: the likelihood is the horseshoe density, the prior distribution is $p(\mathbf{u}, \boldsymbol{\lambda}) = p(\mathbf{u}) \times p(\boldsymbol{\lambda}) = p_1(\mathbf{u})p_2(\mathbf{u}) \times p(\boldsymbol{\lambda})$, and the point estimator for the posterior distribution is the joint posterior-based estimator. In the waterfall region, the performance of the proposed method improves as the number of iterations increases. The method ultimately outperforms the EP method, showing the best results among the compared methods. The improvement in the estimation accuracy with the number of iterations is more pronounced at higher modulation orders. This trend matches the uncoded case, believed to stem from the posterior distribution’s multimodality and HMC’s strong exploration.

Finally, we compare the performance with the SISO AWGN. In Fig. 10, the SISO AWGN plots for the 16QAM and 64QAM scenarios are out of range. Thus, for proper representation, Fig. 11 shows the SISO AWGN performances for all modulation orders. For all modulation orders, the final performance of the proposed method approaches that of the SISO AWGN. For QPSK at 10^{-1} BER, the SNR degradation of our method remains below 1.4 dB. For 16QAM and 64QAM at 10^{-3} BER, it remains below 3.1 and 3.4 dB, respectively. Therefore, even for coded signal detection, our proposed method exhibits near-optimal performance.

VII. CONCLUSION

Employing HMC, t -distribution mixture priors, and horseshoe likelihood, we have developed a signal-detection method capable of delivering near-optimal performance with polynomial complexity. For higher-order modulations, our method significantly outperforms conventional methods in terms of detection performance. Higher-order modulations are poised to play a pivotal role in next-generation wireless networks. Wireless data traffic is expected to surge, driven by multi-sensory interactions surpassing conventional voice and video communication. Consequently, our proposed approach holds significant potential for advancing future wireless technologies.

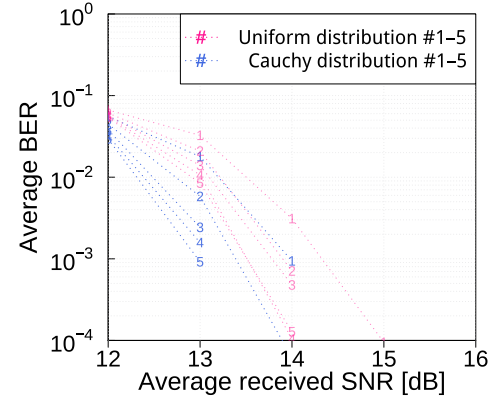


Fig. 12. Performance when λ_n follows a uniform distribution (64QAM).

This research, however, has a limitation that warrants consideration. Although the computational complexity of our method is polynomial, it exceeds that of the EP method. In addition, for coded scenarios with LLR feedback, the iterative improvements of the proposed method come with increased computational costs. Future studies will focus on optimizations to reduce the computational complexity, possibly by leveraging recent advancements in the core sampling mechanisms of the HMC algorithm.

Mathematically, our findings suggest that continuous extensions of discrete problems may yield superior solutions. Our approach could provide valuable insights for continuous relaxation in combinatorial optimization, potentially benefiting classic problems such as the traveling salesman and nurse scheduling problems.

APPENDIX A PERFORMANCE WHEN λ_n FOLLOWS A UNIFORM DISTRIBUTION

Equation (11) considers the multiplier λ_n for the average noise amplitude σ_w as a random variable. We propose that λ_n follows the Cauchy distribution, as shown in (12). Here, we examine the performance when λ_n follows a basic uniform distribution for comparison. Fig. 12 presents the results for the 64QAM scenario, demonstrating that the Cauchy distribution exhibits outstanding performance. This is because the uniform distribution, unlike the Cauchy distribution, leads to unfocused exploration, resulting in inferior estimation performance when computational resources are finite.

ACKNOWLEDGMENT

The authors express their sincere gratitude to Kazushi Matsumura, Hiroki Asumi, and Yukiko Kasuga for their invaluable contributions to this research. They were undergraduate and graduate students at Hokkaido University during the study. Their detailed simulations and valuable technical discussions have significantly enhanced the quality of this study.

REFERENCES

- [1] J. Hagiwara, K. Matsumura, H. Asumi, Y. Kasuga, T. Nishimura, T. Sato, Y. Ogawa, and T. Ohgane, “Near-optimal stochastic MIMO signal detection with a mixture of t -distributions prior,” in *Proc. IEEE Global Commun. Conf. (GLOBECOM)*, Dec. 2023, pp. 6627–6633.

[2] L. Lu, G. Y. Li, A. L. Swindlehurst, A. Ashikhmin, and R. Zhang, "An overview of massive MIMO: Benefits and challenges," *IEEE J. Sel. Top. Signal Process.*, vol. 8, no. 5, pp. 742–758, Oct. 2014.

[3] A. Chockalingam and B. Rajan, *Large MIMO Systems*. Cambridge, UK: Cambridge University Press, 2014.

[4] S. Yang and L. Hanzo, "Fifty years of MIMO detection: The road to large-scale MIMOS," *IEEE Commun. Surveys Tuts.*, vol. 17, no. 4, pp. 1941–1988, Fourth Quarter 2015.

[5] M. A. Albreem, M. Juntti, and S. Shahabuddin, "Massive MIMO detection techniques: A survey," *IEEE Commun. Surveys Tuts.*, vol. 21, no. 4, pp. 3109–3132, Fourth Quarter 2019.

[6] N. Zilberstein, C. Dick, R. Doost-Mohammady, A. Sabharwal, and S. Segarra, "Annealed Langevin dynamics for massive MIMO detection," *IEEE Trans. Wireless Commun.*, vol. 22, no. 6, pp. 3762–3776, Jun. 2023.

[7] K. Matsumura, J. Hagiwara, T. Nishimura, T. Ohgane, Y. Ogawa, and T. Sato, "A novel MIMO signal detection method using Hamiltonian Monte Carlo approach," in *Proc. 24th Int. Symp. Wireless Pers. Multimedia Commun. (WPMC)*, Dec. 2021, pp. 1–6.

[8] —, "A study on signal detection in massive MIMO using MCMC," *IEICE Tech. Rep.*, vol. 120, no. 74, pp. 91–95, Jun. 2020, Paper RCS2020–38 (in Japanese without peer review).

[9] —, "Improvement on signal detection performance with HMC in massive MIMO," *IEICE Tech. Rep.*, vol. 120, no. 298, pp. 7–12, Dec. 2020, Paper RCS2020–135 (in Japanese without peer review).

[10] H. Asumi, J. Hagiwara, T. Nishimura, T. Ohgane, Y. Ogawa, and T. Sato, "A comparison of variational Bayesian and expectation propagation methods for massive MIMO signal detection," *IEICE Tech. Rep.*, vol. 121, no. 72, pp. 7–12, Jun. 2021, Paper RCS2021–30 (in Japanese without peer review).

[11] H. Asumi, Y. Kasuga, K. Matsumura, J. Hagiwara, T. Nishimura, T. Sato, Y. Ogawa, and T. Ohgane, "Comparison of performance and complexity for different search methods in stochastic MIMO signal detection," *IEICE Tech. Rep.*, vol. 122, no. 73, pp. 150–155, Jun. 2022, Paper RCS2022–49 (in Japanese without peer review).

[12] H. Asumi, S. Kakuta, J. Hagiwara, T. Nishimura, T. Sato, Y. Ogawa, and T. Ohgane, "A study on performance improvement of stochastic MIMO signal detection using variational Bayesian methods," *IEICE Tech. Rep.*, vol. 122, no. 357, pp. 30–35, Jan. 2023, Paper RCS2022–213 (in Japanese without peer review).

[13] Y. Kasuga, J. Hagiwara, T. Nishimura, T. Sato, T. Ohgane, and Y. Ogawa, "A study on signal detection using L-BFGS method in massive MIMO," in *Proc. IEICE General Conf.*, Mar. 2022, p. 358, Paper B-5-47 (in Japanese without peer review).

[14] T. Datta, N. A. Kumar, A. Chockalingam, and B. S. Rajan, "A novel Monte-Carlo-sampling-based receiver for large-scale uplink multiuser MIMO systems," *IEEE Trans. Veh. Technol.*, vol. 62, no. 7, pp. 3019–3038, Sep. 2013.

[15] S. Geman and D. Geman, "Stochastic relaxation, Gibbs distributions, and the Bayesian restoration of images," *IEEE Trans. Pattern Anal. Mach. Intell.*, vol. PAMI-6, no. 6, pp. 721–741, Nov. 1984.

[16] J. C. Hedstrom, C. H. Yuen, R.-R. Chen, and B. Farhang-Boroujeny, "Achieving near MAP performance with an excited Markov chain Monte Carlo MIMO detector," *IEEE Trans. Wireless Commun.*, vol. 16, no. 12, pp. 7718–7732, Dec. 2017.

[17] X. Zhou, L. Liang, J. Zhang, C.-K. Wen, and S. Jin, "Gradient-based Markov chain Monte Carlo for MIMO detection," *IEEE Trans. Wireless Commun.*, vol. 23, no. 7, pp. 7566–7581, Jul. 2024.

[18] N. M. Gowda, S. Krishnamurthy, and A. Belogolov, "Metropolis-Hastings random walk along the gradient descent direction for MIMO detection," in *Proc. IEEE Int. Conf. Commun. (ICC)*, Jun. 2021, pp. 1–7.

[19] J. Céspedes, P. M. Olmos, M. Sánchez-Fernández, and F. Pérez-Cruz, "Expectation propagation detection for high-order high-dimensional MIMO systems," *IEEE Trans. Commun.*, vol. 62, no. 8, pp. 2840–2849, Aug. 2014.

[20] T. P. Minka, "Expectation propagation for approximate Bayesian inference," in *Proc. 17th Conf. Uncertainty Artif. Intell. (UAI)*, Aug. 2001, pp. 362–369.

[21] S. Duane, A. Kennedy, B. J. Pendleton, and D. Roweth, "Hybrid Monte Carlo," *Phys. Lett. B*, vol. 195, no. 2, pp. 216–222, Sep. 1987.

[22] M. Girolami and B. Calderhead, "Riemann manifold Langevin and Hamiltonian Monte Carlo methods," *J. R. Stat. Soc. Ser. B. Stat. Methodol.*, vol. 73, no. 2, pp. 123–214, Mar. 2011.

[23] C. M. Carvalho, N. G. Polson, and J. G. Scott, "The horseshoe estimator for sparse signals," *Biometrika*, vol. 97, no. 2, pp. 465–480, Jun. 2010.

[24] B. Hassibi, M. Hansen, A. G. Dimakis, H. A. J. Alshamary, and W. Xu, "Optimized Markov chain Monte Carlo for signal detection in MIMO systems: An analysis of the stationary distribution and mixing time," *IEEE Trans. Signal Process.*, vol. 62, no. 17, pp. 4436–4450, Sep. 2014.

[25] A. E. Hoerl and R. W. Kennard, "Ridge regression: Biased estimation for nonorthogonal problems," *Technometrics*, vol. 12, no. 1, pp. 55–67, Feb. 1970.

[26] C. M. Bishop, *Pattern Recognition and Machine Learning*. New York, NY, USA: Springer, 2006.

[27] A. M. Mussi and T. Abrão, "Mitigating the noisy solution impact of mixed Gibbs sampling detector in high-order modulation large-scale MIMO systems," *EURASIP J. Adv. Signal Process.*, vol. 2021, no. 83, pp. 1–22, Sep. 2021.

[28] A. Kucukelbir, D. Tran, R. Ranganath, A. Gelman, and D. M. Blei, "Automatic differentiation variational inference," *J. Mach. Learn. Res.*, vol. 18, no. 1, pp. 430–474, Jan. 2017.

[29] A. Gelman, J. B. Carlin, H. S. Stern, D. B. Dunson, A. Vehtari, and D. B. Rubin, *Bayesian Data Analysis*, 3rd ed. Boca Raton, FL, USA: CRC Press, 2013.

[30] C. Berrou, A. Glavieux, and P. Thitimajshima, "Near Shannon limit error-correcting coding and decoding: Turbo-codes (1)," in *Proc. IEEE Int. Conf. Commun. (ICC)*, vol. 2, May 1993, pp. 1064–1070.

[31] R. Hayakawa and K. Hayashi, "Convex optimization-based signal detection for massive overloaded MIMO systems," *IEEE Trans. Wireless Commun.*, vol. 16, no. 11, pp. 7080–7091, Nov. 2017.